IEEE Access
Multidisciplinary ⋮ Rapid Review ⋮ Open Access Journal

Received December 18, 2020, accepted January 11, 2021, date of publication January 18, 2021, date of current version January 25, 2021.

Digital Object Identifier 10.1109/ACCESS.2021.3052076

Jamming Efficiency Analysis Based on the Range Profile of Target With Chaff

YANCHUN ZUO, LIXIN GUO, (Senior Member, IEEE), WEI LIU, (Member, IEEE), AND JIANYANG DING, (Graduate Student Member, IEEE)

School of Physics and Optoelectronic Engineering, Xidian University, Xi'an 710071, China

Corresponding author: Lixin Guo (lxguo@xidian.edu.cn)

This work was supported in part by the National Natural Science Foundation of China under Grant 61871457, and in part by the Foundation for Innovative Research Groups of the National Natural Science Foundation of China under Grant 61621005.

ABSTRACT Chaff cloud is widely used in target covering. In this paper, a jamming performance estimation strategy is presented for the elliptical and cubic chaff clouds. The range profiles of the composite models of the plane with the chaff cloud are experimentally accessed in an anechoic chamber using a stepped-frequency waveform measurement system. Then, dimensions, characteristic length, and distributing entropy of the equivalent scattering centers of the plane and the jammer are extracted from the measured range profiles, respectively. Based on these features, support vector machines, naïve Bayesian classification, and decision tree classification methods are employed to determine the recognition rate of the target under the chaff jamming, and then determine the jamming efficiency of the two kinds of chaff clouds. Results show that two types of chaff clouds are able to reduce the target recognition rate. Besides, when the radar uses the Euclidean distance and decision tree classification methods to complete the recognition task, a good jamming efficiency can be achieved by releasing the elliptical or the cubic chaff cloud. Meanwhile, a low level of jamming performance outcomes using the support vector machines classification method. It is also found that the chaff cloud released from the side of the plane achieves a better jamming performance compared with the other releasing locations. Finally, the influence of environmental noise on the recognition rate of the plane is studied. Estimating results show that the recognition rates decrease with the increasing of the power level of the noise. When the transmitting power level of the noise reaches 1.2 times the reflected power level of the target, it is quite hard to estimate the jamming performance of two kinds of chaff clouds.

INDEX TERMS Range profile, target recognition, chaff cloud, jamming performance analysis.

I. INTRODUCTION

Chaff cloud is widely used in electronic countermeasures since the Second World War [1]. Targets release the chaff cloud to confuse the radar and it increases the survival rate of the target. In practical applications, huge numbers of the chaff elements are employed to pursue a large Radar Cross Section (RCS) for target covering. There are mainly two types of chaff clouds that are frequently used in practice: ellipsoid shaped chaff cloud and chaff corridor. In order to make the most use of the chaff cloud, estimating the jamming efficiency of the chaff cloud before it is put into tactical use is strongly demanded.

The jamming efficiency estimation of the chaff cloud starts with the electromagnetic (EM) scattering evaluation of the chaff cloud [2]–[4]. Such research generally follows three technical routes, i.e., calculate the EM scattering of the target and jammer using analytical, numerical, and experimental strategies. Analytical methods can efficiently evaluate the scattering of large scale chaff cloud. However, the couplings between chaff elements in the cloud are always neglected, which causes inaccurate estimation results. To incorporate the EM coupling effect in scattering evaluation, numerical methods are usually used in the related works [5]–[9]. In this calculation strategy, the basis functions are defined on the surface of the chaff elements. This results in a large-scale matrix equation, which contains large numbers of unknowns, according to Maxwell's equations. Solving such a large-scale matrix equation may produce a considerable computational load. In some cases, even a supercomputer is unable to find the solution of this matrix equation within a reasonable amount of time. Some researchers also use experimental

The associate editor coordinating the review of this manuscript and approving it for publication was Guido Valerio.

methods to investigate the scattering properties of the chaff cloud. In the test, a target tracking radar is utilized to monitor and record the echo of the chaff cloud [10]–[12]. Then, the collected data is processed to acquire the scattering characteristics of the chaff cloud. The limitation of the experimental methods is that outdoor experiments are always unable to cover all the application scenarios due to the influence of stochastic factors. Moreover, the outdoor aerodynamic and scattering experiments related to the chaff cloud are conducted at high cost. Even so, experiments still provide an efficient way to study the EM scattering of the chaff cloud, which takes into account complex factors that are not fully considered in the theoretical studies.

Based on the EM scattering results of the chaff cloud and the target, researchers analyze the jamming performance of the chaff cloud in different application scenarios [11], [13]–[15]. When the chaff cloud is released by a high-speed carrier, Doppler effect analysis is always performed to distinguish the high-speed target from the chaff cloud. Because the speed of the chaff cloud decreases sharply after it is released by the high-speed carrier. However, various diffusion conditions cause a large frequency fluctuation in Doppler domain, which makes the target recognition depending on the Doppler analysis not always a reliable way. Furthermore, when the chaff cloud emerges with the slow-small target, it is harder to ''pick out'' the target under the chaff jamming. Some researchers also conduct the target recognition task applying the range profile examination which is related to the geometric characteristics of the target [16]–[22]. The features for recognition of the target are extracted from the range profiles and compared with that of a labeled target in the database. Nevertheless, most of these target recognition strategies are carried out without consideration of the chaff jamming. Besides, the jamming efficiency estimation of the chaff cloud is rarely addressed in the open literature.

To tackle the remained issues mentioned above, we put forward the following technical routes which are also the key contributions of this paper.

(i) Experimentally determines the range profile of the plane with the chaff cloud. Although lots of researchers devote their efforts to obtain the range profiles of the target, there are still quite a few published works that focus on the studying of one-dimensional imaging methods for the plane coexists with the chaff cloud owing to heavy EM computational loads. To overcome this obstacle, indoor scattering measurements are performed in this paper to obtain the scattering fields of the composite model of the chaff cloud with the plane at discrete frequency points using a stepped-frequency waveform measurement system. Then, the range profiles of the composite model at different observation angles are determined just by using the fast Fourier transform (FFT) algorithm. This measurement strategy provides an efficient way to access the range profiles of complex models with the consideration of complex EM couplings that are involved in the chaff cloud and between the plane and chaff cloud.

(ii) Jamming efficiency evaluation and better use of the chaff cloud. Most of the opened works concentrate on the EM scattering evaluation of the chaff cloud without the presence of the target. In real-world application scenarios, the chaff cloud always appears together with the target within a resolution cell. Thus, studying the scattering properties of the chaff cloud independently is unreasonable. Regrading the jamming efficiency estimations as well as the tactical use of the chaff cloud, fewer achievements are reported. To improve this problem, three feature extraction methods and four classification algorithms are employed in this paper to estimate the jamming performance of the chaff cloud in the scenario of air campaigns. We also provide an optimized releasing strategy of the chaff cloud which can be used to achieve a better jamming performance.

(iii) An accurate physical model making scheme of the chaff cloud. There are only a few published works that studied the physical modeling techniques for the chaff cloud according to the simulation one. Because large numbers of the chaff elements are discretely distributing in the free space. This results in a high making complexity in fixing the chaff elements one by one on a supporting material. Furthermore, if the physical model of the chaff cloud is handmade, it cannot meet the accuracy requirement of the experiment in most test scenarios. To solve this problem, we first divide the simulation model of the chaff cloud into several cubes on a computer. Then, the chaff elements are inserted into low-radar cross section (low-RCS) cubes in order according to the divided chaff cloud model with the help of a specific insertion machine. This proposed strategy provides an efficient and accurate way to perform a controllable test for obtaining the EM scattering of the chaff cloud.

The rest of this paper is organized as follows. Section II discusses the related work. Section III details the geometric and physical model generation methods for the chaff cloud. The range profile measurement principle of the chaff cloud with the plane is then addressed. Based on the range profiles, the feature extraction and jamming efficiency estimation methods are detailed in Section IV. The experiments and analyses are finally presented in Section V followed by conclusions in Section VI.

II. RELATED WORK

The studies of the chaff cloud are conducted from two aspects. One is developing accurate and efficient EM scattering evaluation algorithms. The other is the jamming efficiency estimation of the chaff cloud based on the obtained EM scattering data. The related work discussed below is centered around these two points.

A. SCATTERING EVALUATION OF THE CHAFF CLOUD

The EM scattering evaluation of the chaff cloud is the prerequisite of the jamming efficiency analysis. Li *et al.* performed the force analysis of a single chaff element in thin air. Then, a motion model of the chaff cloud was established following the kinetic equations, Mote-Carlo methods,

and the motion characteristics of a single chaff element. Based on the obtained geometric models, an RCS decay model of the chaff cloud was accessed. Furthermore, the covering time of the chaff cloud was also analyzed [8]. Chen *et al*. gave a surface current formula for any length chaff element according to the lag potential principle in EM theory. Besides, they obtained the statistical properties of the RCS utilizing a multi-zone basing point algorithm [7]. Li *et al*. analyzed the polaristic EM scattering properties of the chaff clouds with different cloud shapes and different probability density functions of the orientation and central coordinate of the elements with the help of numerical methods [3]. Marcus *et al*. calculated an average bistatic RCS of a spherical chaff cloud. Marcus suggested that the total EM scattering of the chaff cloud is the sum of incoherent and coherent scattering contributions of chaff elements [2]. Hu *et al*. compared the far-field radiation pattern of the actual chaff element with the ideal dipole based on the method of moments (MoM). The length reduction effect was found. Meanwhile, the formula of averaged RCSs of single chaff element in the single-station and bi-station were calculated [5]. Yang *et al*. compared the RCSs of three kinds of chaff clouds using the MoM. They found that the EM couplings between chaff elements are weak and can be neglected unless the averaged distance between elements is larger than two times the length of the operating wavelength of the radar [6]. Cheng *et al*. designed a chaff element by changing the surface current distributions of the element using specific structures in the millimeter band. Then, the genetic optimization algorithms combined with MoM were carried out to improve the structure designing of the chaff element, which achieved a better jamming performance [9]. All the mentioned schemes provide ways to access the EM scattering properties of the chaff cloud. However, all of these evaluation schemes cannot balance the contradiction between computational accuracy and efficiency.

Some researchers also use experiments to investigate the scattering properties of the chaff cloud in practice. Wang *et al*. studied the separation and dispersion characteristics of the chaff cloud launched at high-speed. It was found that the radial number of chaff elements increases and the onset jamming time of the chaff cloud delays with the rise of the velocity of the carrier. Moreover, they pointed out that the number of radial elements does not linearly increase with the increment of the carrier velocity [12]. Huang *et al*. established a multi-chaff kinetic model to experimentally analyze the holistic kinetic performance of the chaff cloud under the impact of high-speed airflow. They found that the aerodynamic interferences between elements are mainly related to the overlapping area and the distance among chaff elements during the diffusion process. Their simulation results also show that the chaff elements fully diffuse under the impact of high-speed airflow within 0.5 s. Furthermore, the shape of the chaff cloud is similar to a cone that forms a certain angle with the horizontal plane, and most of the chaff elements are clustered around the second half of the cone [23]. According to these achievements mentioned above, it is an efficient way to study the diffusion and EM scattering properties of the chaff cloud by experiments. These strategies can take into account many complex factors that are not fully considered in theoretical methods. Nevertheless, none of these works mentioned above supplies controllable physical model-making strategies and experimental EM scattering estimation schemes of the cloud, which poses a dilemma in obtaining the EM scattering data of the chaff cloud.

B. JAMMING PERFORMANCE ESTIMATING OF THE CHAFF CLOUD

To investigate the jamming performance of the chaff cloud, Winchester *et al*. developed a numerical technique to obtain the statistical characteristics of the pulsed radar that returns from a chaff cloud. They found that the echo power of the chaff cloud follows Gaussian distribution because of the nonlinear summation of the echoes reflected by the chaff elements [11]. Gan *et al*. studied the influence of the geometric attributes of the chaff cloud, i.e., the length, width, and thickness of the chaff block, on the radar echo [15]. They concluded that the shape of the chaff cloud extremely affects the echo characteristics of the chaff cloud, which can be utilized to distinguish the chaff corridor from the target. Their efforts all concentrate on obtaining the statistical characteristics of the chaff cloud without the existence of the target.

Regarding the jamming efficiency estimation of the chaff cloud, Shao *et al*. pointed out that it is difficult to recognize the chaff cloud in both time and frequency domain. They recommended that the recognizing task can be fulfilled in the polaristic domain according to a known RCS spectrum of the chaff cloud [4]. Guo *et al*. studied the characteristics of the range profile of the chaff cloud using a BP neural network and designed a classifier to recognize the ongoing chaff jamming [24]. Luo *et al*. recognized the target by comparing and analyzing the angle similarity of this target with a labeled one stored in the database. The angle similarity of two targets is determined based on the generalized information cut of the range profiles of these two targets. This similarity comparing strategy improves the automatic target recognition rates [17]. Li *et al*. studied the problem that hyperspectral images (HSIs) contain large amounts of noise, which hampers the target recognition process. They introduced a method to reconstruct the HSI with noise reduction and contrast enhancement strategies using a matting model [18]. Dung *et al*. proposed a method to recognize the radar targets from radar range profiles with the help of neural networks [16]. Batı *et al*. introduced a classification method using the information fusion algorithm for target identifications, which reduces the influence of the environment changes on the recognition process [19]. Lu *et al*. used a technique for the recognition of ship targets based on the high resolution range profile data, which incorporates Fourier-Mellin transform and support vector machine method to achieve the ship identification [20]. Li *et al*. declared an algorithm based on cross-range profile to estimate the size of space-target by single range cell motion compensation and cross-range scaling, which can be

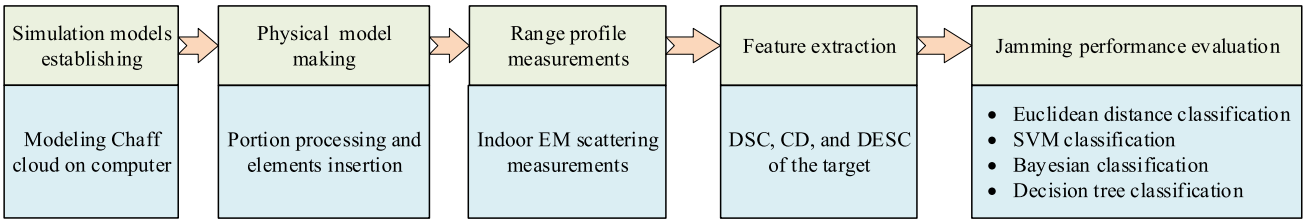

FIGURE 1. The flow chart of the jamming performance evaluation.

used to monitor the collision of space targets [21]. Zhu *et al*. estimated the special distribution characteristics of the echoes received by a stepped-frequency radar system under the condition of range ambiguity [22]. The achievements listed above perform the jamming efficiency analysis and the target recognition directly using the range profiles of the chaff cloud and the target. However, the envelops of the target and the chaff cloud are always similar to each other, which makes it hard to develop the jamming efficiency analysis abilities of these methods.

To make full use of the information involved in the range profiles, some features related to the target and the chaff cloud should be extracted. In theory, the range profile is considered as the coherent summations of the complex time returns from scatters located in different range cells. In other words, the range profile represents the projection of the complex electric fields scattered by separated equivalent scattering centers onto the radar line-of-sight [25]. Schuler *et al*. proposed a method to extract the scattering centers of the target using the ray-tracing EM scattering evaluation method [26]. Pei *et al*. presented a method of airplane-like target recognition according to the information taken from the high- resolution radar echoes using the Relax algorithm [27]. June *et al*. addressed a method to retrieve the real target using the data on the major axis of the scattering center pattern in synthetic aperture radar images. The similarity of the two targets is determined by measuring the Hausdorff distance between two range profiles [28]. Wang *et al*. dealt with the target recognition problem making use of the power entropy that is widely adopted in the description of the dispersion of the scattering centers [29]. Potter *et al*. presented a method for feature extraction from the radar returns which are calculated by the geometrical theory of diffraction. Then, the statistical characteristics of these features are evaluated [30]. Wang *et al*. put forward a multi-target tracking strategy based on information fusion theory. Specifically, an online multi-target tracking method is introduced to generate reliable track in real-time [31]. Bai *et al*. proposed a target tracking algorithm based on entropy penalized expectation maximization of the unknown clutter estimations [32]. Zhu *et al*. investigated the anti-chaff jamming strategy utilizing the Doppler profile of the target. Several characteristic parameters related to the target are extracted. Then, an identification method based on these extracted parameters was presented to discriminate the chaff jamming from the ship [14]. Yan *et al*. also proposed a chaff-jamming countermeasure method based on the geometrical inference matching algorithm which reduces the influence of the chaff jamming on the true target's tracking by terminal guidance radar [13]. Most of these achievements mentioned above concentrate on the recognition of the target(s) without chaff jamming and the jamming countermeasure methods. Few works are published to deal with jamming efficiency estimation of the chaff cloud and the optimized tactical use of the chaff cloud.

III. MODELING AND MEASUREMENT METHOD

In this paper, a two-steps scheme is adopted to perform the jamming efficiency estimation of the chaff cloud. In the first step, the simulation and physical modeling strategies of the chaff cloud are proposed. Then, the EM scattering evaluation method of the chaff cloud existing with the plane is studied. For the second step, the jamming efficiency of the chaff cloud is estimated utilizing four classification methods. The block diagram of these processes is shown in Fig.1. In this section, the methods of simulation and physical modeling of the cubic and elliptical chaff cloud are presented. Statistical approaches are carried out to describe the spatial distribution and orientation characteristics of the chaff elements. Then, a specific insertion machine is designed to make the physical models of the chaff cloud. At last of this section, we discuss the theorem for range profile measurement.

A. MODELING OF THE CHAFF CLOUD

The attitude of a chaff element in the atmosphere can be characterized by both its central coordinate and orientation. To mathematically express these two spatial attributes, two coordinate systems are created as shown in Fig.2.

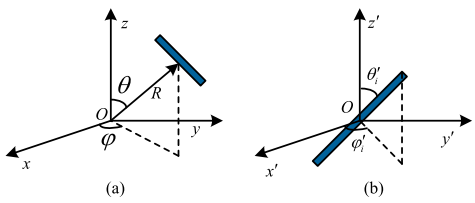

FIGURE 2. The coordinates system for the chaff cloud.

The global coordinate system is shown in Fig.2 (a), in which its origin is fixed on the geometric center of the calculation region. The local coordinate system is illustrated

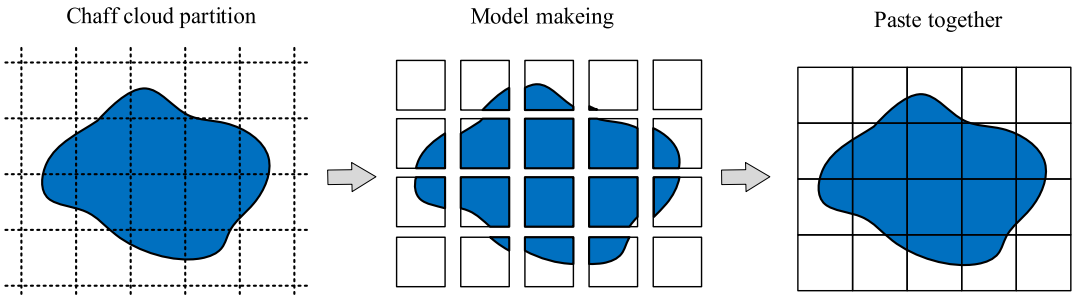

FIGURE 3. The making process of the chaff cloud.

in Fig.2 (b), in which the origin of this system is located on the geometric center of each chaff element. Furthermore, the corresponding x'-, y'-, and z'-axis in the local coordinate system are parallel to that of the global coordinate system.

1) CUBIC CHAFF CLOUD MODELING

The cubic chaff cloud, known as the chaff corridor, is frequently employed in many battle scenes. The distributions of the central coordinates, (x_i, y_i, z_i), and the orientations, (θ_i', φ_i'), of the chaff elements can be generally described with the uniform distribution [15], [33]. Then, we have

$$\begin{cases} x_i = x_{\min} + (x_{\max} - x_{\min}) \cdot \text{rand}() \\ y_i = y_{\min} + (y_{\max} - y_{\min}) \cdot \text{rand}() \\ z_i = x_{\min} + (z_{\max} - z_{\min}) \cdot \text{rand}() \end{cases}, \quad \begin{cases} \theta_i' = \pi \cdot \text{rand}() \\ \varphi_i' = 2\pi \cdot \text{rand}() \end{cases} \tag{1}$$

where function rand() can generate a uniformly distributed random number within the interval [0, 1] using Marsaglia-Zama algorithm and acceptance-rejection method [34], [35]. Constants $x_{\min}$, $y_{\min}$, and $z_{\min}$ give the lower central coordinates bound and $x_{\max}$, $y_{\max}$, and $z_{\max}$ give the upper central coordinates bound of the chaff elements in the Cartesian coordinate system. For creating all the elements in the chaff corridor. One just needs to repeat the generation process according to (1).

2) ELLIPTICAL CHAFF CLOUD MODELING

When the chaff elements are released by an explosive, the shape of the chaff cloud commonly appears as an elliptical-like object. In addition, the distance between the geometric center of the chaff element and the origin of the global coordinate system obeys normal distribution [36]. Similar to the cubic chaff cloud, the central coordinate, say (x, y, z), of the chaff element is mathematically expressed as

$$\begin{cases} x = R_x \cdot \sin\theta \cdot \cos\varphi \\ y = R_y \cdot \sin\theta \cdot \sin\varphi \\ z = R_z \cdot \cos\theta \end{cases}, \quad R \sim N(R_0, \sigma^2) \tag{2}$$

where R_x, R_y, and $R_z$are the principal semi-axes length of the chaff cloud along x, y, and z directions. Angles θ and φ are the azimuthal and zenith angles in spherical coordinate system coexisting with the global Cartesian coordinate system, which can be seen in Fig.2 (a). R denotes the distance between the origin and the geometric center of the chaff element. The symbol$N(R_0, \sigma^2)$ represents the probability density function of the normal distribution with mean R_0 and standard deviation σ. Same to the cubic chaff cloud, the central coordinate and the orientation of each chaff element can be generated one by one using Marsaglia-Zama and acceptance-rejection methods.

3) PHSICAL MODEL MAKING STRATEGY

After developing the simulation models, we now discuss how to make the physical model of the chaff cloud according to the simulation one. It is noteworthy that if the physical model of the chaff cloud is manually made, it is quite hard to achieve an efficient element insertion process. Meanwhile, it is also hard to produce a chaff cloud model with satisfactory manufacturing accuracy. Thus, in this paper, we perform four steps model making processes as follows:

Step 1: The simulation model is divided into several parts as shown in Fig.3. The 3D rectangular mesh is adopted for the convenience of the physical model making.

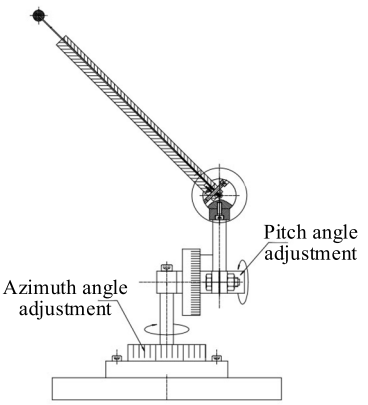

FIGURE 4. Insertion mechanism.

Step 2: The simulation data, i.e., the central coordinates and orientations of the chaff elements, is exported from the computer. These data are then used to guide the machine to insert the metallic fibers into the low-RCS material. The core structure of this machine is the insertion mechanism shown in Fig.4. The mechanism adjusts the pitch and azimuth angles

of the insertion passage according to exported data. Once the insertion direction is confirmed, the elements are pushed into the low-RCS blocks in front of the insertion passage. To improve the insertion efficiency, a track is added into the system associating with the insertion mechanism, which can be seen in Fig.5.

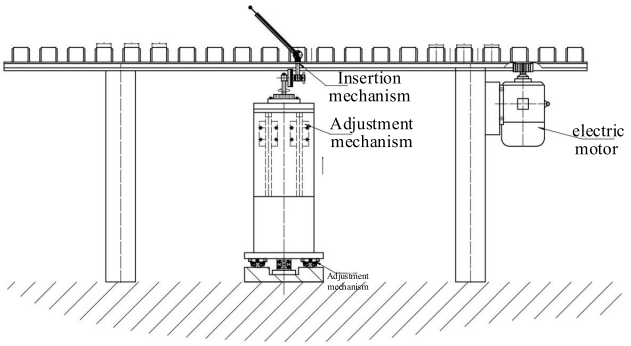

FIGURE 5. Elements insertion machine.

Step 3: After all the blocks are inserted with the elements, these blocks are put together to make up a physical model of the chaff cloud.

When all the making steps presented in this section are conducted, the simulation and physical models of the chaff cloud are established. This physical model making strategy provides a controllable way to create the model of the chaff cloud. It should be emphasized that numbers of the chaff cloud samples under the same experimental condition are made and submitted to the measurement process. Then, the scattering properties of the chaff cloud are obtained by statistically averaging the results accessed in each round of test.

B. RANGE PROFILE MEASUREMENTS

In this subsection, the principle how to measure the range profile of the chaff cloud and the plane based on the stepped-frequency waveform (SFW) system is introduced. The SFW is able to provide a large total bandwidth for high range resolution by sequentially changing the carrier frequency over pulses [37]. The sub-pulses of the SFW are [38]

$$s_i(t) = \begin{cases} u(t)A_i e^{j(2\pi f_i t+\theta_i)} & iT_r - \dfrac{T}{2} \le t \le iT_r + \dfrac{T}{2} \\ 0 & \text{else} \end{cases} \quad (3)$$

where $u(t)$ is the envelope of sub-pulse, A_i and θ_i are the initial amplitude and phase respectively, T_r is the pulse repetition period, T is the duration of sub-pulse. f_i is the carrier frequency of each sub-pulse defined as

$$f_i = f_0 + i\Delta f, \quad i = 0, 1, 2, \ldots, N-1 \quad (4)$$

where f_0 is the initial carrier frequency, Δf is step size of carrier frequency, i is the index of sub-pulses. Yang *et al.* also gave the range resolution Δr as

$$\Delta r = \frac{c}{2B_w} \quad (5)$$

where c is the speed of light, B_w is bandwidth of the SFW. Then, the transmitting SFW is given by

$$s(t) = \sum_{n=0}^{N-1} u(t - nT_r)e^{i2\pi f_n t} \quad (6)$$

Let the scattering coefficients of scattering centers of the target as $\rho_m = B_m e^{j\phi_m}$, then the echo of the target is

$$R(t) = \sum_{m=1}^{M} B_m e^{j\phi_m} \otimes s(t) \quad (7)$$

where, the symbol $\otimes$ denotes convolution operation. The range profile of the target can be readily created by calculating IFFT of (7). Then, we obtain

$$HRRP(k) = \sum_{m=1}^{M} B_m \left| \frac{\sin\left[\pi\left(k - N\Delta f \frac{2R_m}{c}\right)\right]}{\sin\left[\frac{\pi}{N}\left(k - N\Delta f \frac{2R_m}{c}\right)\right]} \right| \quad (8)$$

This formula takes the maximal value at

$$k_p = N\Delta f \frac{2R_m}{c} \quad (9)$$

where R_m is the distance from the radar to the m-th scattering center. Thus we have

$$R_m = \frac{c}{2N\Delta f} k_p \quad (10)$$

Finally, one can determine the location of the equivalent scattering centers of the target and the chaff cloud by finding the abscissa values of the peaks in (8).

IV. JAMMING PERFORMANCE ESTIMATION THEORY

After determining the range profile of the chaff cloud and the plane existing with the chaff cloud, three attribute extraction methods are utilized in this section to describe the geometric features of the target and jammer. Then, four classification methods are applied to perform the jamming efficiency estimation of the chaff cloud based on the obtained features. The flowchart of the process is illustrated in Fig.1.

A. FEATURE EXTRACTIONS

The features extracted from the range profiles should reflect the geometric differences of the plane with the jammer [39]. In view of this, three features are selected. The first one is the dimensional scale of the scattering centers (DSC). The second one is the characteristic length (CL) of the target, and the third one is the distributing entropy of the scattering centers (DESC). These features are detailed as follows.

1) DSC OF THE RANGE PROFILE

The EM scattering of a target is approximately regarded as the summation of the scattering produced by a few scattering centers [40]. Hence, the number of the scattering centers are closely related to the geometric configurations of the target and the jammer. Moreover, the DSC of the range profile is sensitive to the chaff jamming, which makes it an appropriate feature to illustrate the influence of the chaff jamming on

target recognition. It also makes the DSC of the range profile a felicitous feature to describe the jamming efficiency of the chaff cloud.

Four threshold values are firstly determined to find the useful part of the range profile, which are shown in Fig.6. $rpc_{\min}$ and $rpc_{\max}$ determine the window size of the testing region we are interested in. Besides, $amp_{\min}$ and $amp_{\max}$ are determined by the level of the background noise, the sensitivity of the instruments, and the maximum reflected power of the object under test. After obtaining these four parameters, the range profile of the object (blue region in Fig.6) is picked out and denoted as $RP(m\Delta r)$, where Δr is the sampling interval of the range profile and $m = 0, 1, \ldots, M$. In a subsequent descriptions, the range profile $RP(m\Delta r)$ is rewritten as $RP(m)$ for convenience with the consideration of the fact that Δr is a constant.

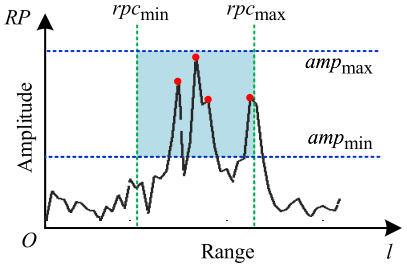

FIGURE 6. Dimensional scale determination.

The next step is determining the dimensional scale of the range profile $RP(m\Delta r)$ by means of comparing the values of $RP(m+1)$, $RP(m-1)$ and $RP(m)$. Scan all the values of the range profile. If the criterion

$$RP(m+1) < RP(m) > RP(m-1) \tag{11}$$

is met, the peak number $feature_{DSC}$ pluses 1. Meanwhile, the abscissas of these peaks are recorded. After all the values of the $RP(m)$ are traversed, the dimensional scale of the range profile, i.e., $feature_{DSC}$, is determined.

2) CL OF THE RANGE PROFILE

The CL, say $feature_{CD}$, is an important feature of the target and the jammer. It measures the propagation width of the object onto the radial direction of the radar. The usage of the chaff cloud expands the CL of the range profile of the target and thus realizes passive jamming. Therefore, the CL of the range profile can be adopted to characterize the jamming performance of the chaff cloud.

In the former discussion, the abscissas of the range profile peaks are recorded. The maximum and minimum abscissas of the peaks can be determined and denoted as $L_{\max}$ and $L_{\min}$, respectively. Thus, the value of $feature_{CD}$ is calculated as

$$feature_{CL} = L_{\max} - L_{\min} \tag{12}$$

The image of the determination of CL is shown in Fig.7.

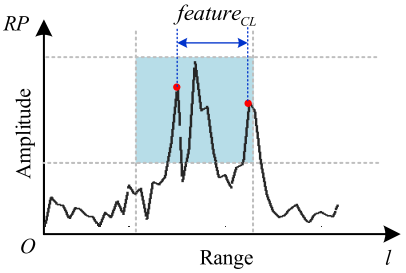

FIGURE 7. The image of the characteristic dimension.

3) DESC OF THE RANGE PROFILE

Entropy is a measure of randomness or disorder of a system [41]. In this paper, the entropy is introduced to describe the concentration of the scattering centers of the target and the jammer. Besides, the chaff cloud significantly influences the entropy of the scattering centers and thus affects the target recognition. Therefore, the DESC can be selected as a feature to characterize the jamming efficiency of the chaff cloud. To calculate the entropy, normalization of the range profile is first performed as follow

$$\overline{RP}(m) = \frac{RP(m)}{\sum_{m=1}^{M} RP(m)} \tag{13}$$

Then, the entropy of the range profile is expressed as

$$feature_{DESC} = -\sum_{m=1}^{M} \overline{RP}(m) \cdot \log_{10}(\overline{RP}(m)) \tag{14}$$

B. JAMMING EFFICIENCY ESTIMATION OF THE CHAFF CLOUD

Before performing the estimation process, the test scenarios are first introduced in this subsection, which is designed according to the real application strategies of the chaff cloud. Then, four methods are presented to evaluate the jamming efficiency of the chaff cloud.

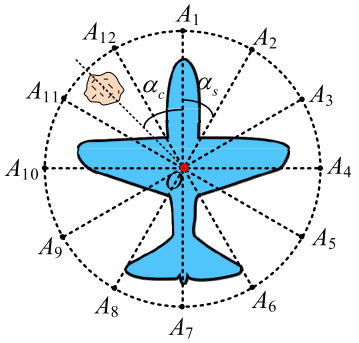

FIGURE 8. The directions of obtaining the range profile.

The plane with a chaff cloud is placed on the upper surface of a turntable, see Fig.8. The range profile of this composite model is measured along direction $\overrightarrow{A_1O}$, $\overrightarrow{A_2O}$, $\overrightarrow{A_3O}$, etc.

The test positions (A_1, A_2, A_3, etc.) are uniformly located on the test circle. The corresponding sampling angles are denoted as $\alpha_s^{(1)}$, $\alpha_s^{(2)}$, etc. Meanwhile, the location of the chaff cloud is measured by angle α_c. After conducting the measurements, the range profiles of the chaff cloud, plane, and the chaff cloud plane are accessed at different α_c's.

1) METHOD 1: EUCLIDEAN DISTANCE CLASSIFICATION

Euclidean distance is the distance between two points in Euclidean space. As described above, three features of the range profiles are extracted. Accordingly, each range profile corresponds to a three-dimensional point in Euclidean space. The coordinates of this point are determined by the values of the DSC, CL, and DESC of the range profile. We define this Euclidean space as $\mathbb{R}_e^3$. If the range profiles of the plane with or without the chaff jamming are more similar to each other, the Euclidean distance between these two points is shorter [42]. This makes it more difficult to recognize the target under chaff jamming. In contrast, a larger Euclidean distance increases the identification probability of the plane. This indicates a lower jamming efficiency. Given this, we introduce a jamming efficiency estimation algorithm based on the Euclidean distance. The estimation steps are described as follows

Step 1: The range profiles of the plane and the chaff cloud are measured along the directions illustrated in Fig.8. The coordinates of these range profiles in $\mathbb{R}_e^3$ are determined by calculating their corresponding DSCs, CLs, and DESCs. We denote the coordinate of the i-th point for plane in feature space $\mathbb{R}_e^3$ as $(p_1^t(i), p_2^t(i), p_3^t(i))$. Likewise, the coordinate of the chaff cloud is $(p_1^c(i), p_2^c(i), p_3^c(i))$.

Step 2: If the number of the range profile slices of the ship and the chaff cloud in Step 1 is M. The cluster centers, i.e., the "gravity centers", of the plane $(C_1^{plane}, C_2^{plane}, C_3^{plane})$ and the chaff cloud $(C_1^{chaff}, C_2^{chaff}, C_3^{chaff})$ are

$$\begin{cases} C_1^{plane} = \dfrac{1}{M}\sum_{i=1}^{M} p_1^t(i) \\ C_2^{plane} = \dfrac{1}{M}\sum_{i=1}^{M} p_2^t(i) \\ C_3^{plane} = \dfrac{1}{M}\sum_{i=1}^{M} p_3^t(i) \end{cases}, \quad \begin{cases} C_1^{chaff} = \dfrac{1}{M}\sum_{i=1}^{M} p_1^c(i) \\ C_2^{chaff} = \dfrac{1}{M}\sum_{i=1}^{M} p_2^c(i) \\ C_3^{chaff} = \dfrac{1}{M}\sum_{i=1}^{M} p_3^c(i) \end{cases} \tag{15}$$

These two points are used as a classification reference in $\mathbb{R}_e^3$ to determine which class the test range profile belongs to.

Step 3: The range profiles of the plane with the chaff cloud are also measured as shown in Fig.8. Being same to the Step 1, the coordinates of these range profiles in the feature space are obtained and denoted as $(p_1^{tc}(i), p_2^{tc}(i), p_3^{tc}(i))$. The distances from these points to two classification reference centers are determined as (16) and (17), as shown at the bottom of the next page. If $d_1^i > d_2^i$, the value of successful identification number N_{suc} pluses 1. Otherwise, no action is taken. After all the range profiles of the plane with chaff cloud are traversed, the recognition rate R_{rec} is determined as

$$R_{rec} = \frac{N_{suc}}{M} \times 100\% \tag{18}$$

according to the value of R_{rec}, the jamming efficiency of the chaff cloud can be determined. The flowchart of this process is illustrated in Fig.9.

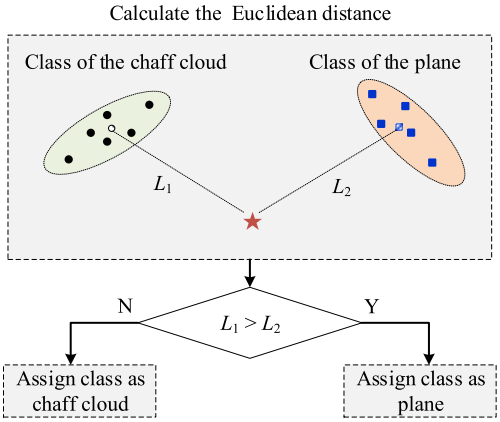

FIGURE 9. The diagram of the Euclidean distance classification.

2) METHOD 2: SVM CLASSIFICATION

Support vector machine (SVM) is a powerful supervised machine learning algorithm used in classification problems. The goal of SVM is to divide the datasets into classes to find a maximum marginal hyperplane. The details of this method can be found in literature [43]–[45]. Here, we use this method to perform plane recognition under the chaff jamming.

Similar to the strategies in Method 1, the range profiles of the plane, chaff cloud, and plane with chaff cloud along different directions are measured. Then, the features of each range profile are extracted using the methods explained in part A of Section III. Next, the coordinates of the range profiles in the feature space are determined and form the training set. Correspondingly, the test set consists of the coordinates of the range profiles of the plane with chaff cloud. We set the class label of the plane as 1, and the label of the chaff cloud as 0. In addition, the feature sets of the plane and the chaff cloud are denoted as D_1 and D_2 in the feature space, respectively. The coordinates of all the points in these two sets are denoted as $(p_1^t(i), p_2^t(i), p_3^t(i))$. A parameterized plane $\mathbf{wp}' + \gamma = 0$ is selected to divide the data space into two subdomains with the minimum classification errors. Thus, we have

$$\begin{aligned} \tilde{D}_1 &= \{\mathbf{p} : \mathbf{wp}' + \gamma \le 0\} \\ \tilde{D}_2 &= \{\mathbf{p} : \mathbf{wp}' + \gamma > 0\} \end{aligned} \tag{19}$$

The symbol $\mathbf{p}'$ denotes the transposes of the vector $\mathbf{p}$. Sets $\tilde{D}_1$ and $\tilde{D}_2$ are possible classification results for all the points in the feature domain. Then the labels of the set $\tilde{D}_1$ and $\tilde{D}_2$ are determined according to the majority rule, i.e., if most of the points in set D_1 are labeled by "1", the label of set D_1

is marked by "1" and vice versa. The same process can be conducted for D_2. Without loss of generality, we labeled $\tilde{D}_1$ as "plane" and labeled $\tilde{D}_2$ as "chaff cloud." The parameter selection process of $\mathbf{w}$ and γ is terminated if the following criteria is met.

$$\min_{\mathbf{w},\gamma} (err_{D1} + err_{D2}) \tag{20}$$

where

$$err_{D1} = \frac{card\left(\left\{\mathbf{p}|\mathbf{p} \in D_1, \mathbf{p} \in \tilde{D}_2\right\}\right)}{card(D_1)} \tag{21}$$

$$err_{D2} = \frac{card\left(\left\{\mathbf{p}|\mathbf{p} \in D_2, \mathbf{p} \in \tilde{D}_1\right\}\right)}{card(D_2)} \tag{22}$$

The function $card()$ returns the element number of the set. After the optimization, the optimized values of $\mathbf{w}_{best}$ and γ_{best} can be determined. The support vector is then determined. Subsequently, the range profile of the chaff cloud with plane is classified according to the obtained support vector. We count the number of the data with Label 1, and denote it as N_{suc}. The total number of the samples in test set is also denoted by M. The recognition rate R_{rec} is then obtained by (18). The above steps are shown in Fig.10. Note that we just use linear kernel function in our method.

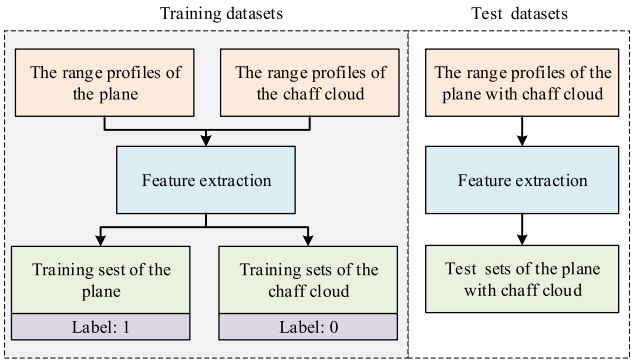

FIGURE 10. The training and test sets.

3) METHOD 3: NAÏVE BAYESIAN CLASSIFICATION

Bayesian classifiers are the statistical classifiers which predict class membership with probability that a given tuple belongs to a particular class, see [46], [47] for details. We have two training sets: one is plane, say set D_1, and the other is the chaff cloud, say set D_2. The label of set D_1 (or D_2) is 1 (or 0). At the training stage, Bayesian classifiers are generated by calculating the frequency of the occurrence of each class and the conditional probability of each class for each attribute. According to Bayesian's law

$$P(y_i|\mathbf{p}) = \frac{P(\mathbf{p}|y_i) \cdot P(y_i)}{P(\mathbf{p})} \tag{23}$$

where y_i is the predicted class that the test range profile belongs to, and $\mathbf{p}$ is a dependent vector which is formed according to the features extracted from the range profiles of the plane and chaff cloud by employing the method presented in part A of Section III. Thus, the feature vector $\mathbf{p}$ can be written as

$$\mathbf{p} = (p_1, p_2, p_3) \tag{24}$$

After formula derivation, the conditional probability on the left hand of (23) can be written as

$$P(y_i|\mathbf{p}) \propto P(y_i) \prod_{m=1}^{3} P(p_m|y_i) \tag{25}$$

The values of $P(y_i)$ and $P(p_m|y_i)$ can be estimated by using Maximum A Posteriori (MAP) method. In general, the values of the DSCs, CLs, and DESCs of the plane and chaff cloud always follow the normal distributions. Thus, the maximum likelihood estimation method is used to determine the values of the mean μ and standard deviation σ of the distribution. Thus, the conditional probability density functions $f(p_m \mid y_i)$ of $P(p_m|y_i)$ at the right hand side of (25) are

$$f(p_i \mid y) = \frac{1}{\sqrt{2\pi\sigma^2}} \exp\left(-\frac{(x_i - \mu)^2}{2\sigma^2}\right) \tag{26}$$

Subsequently, the probability of given set of inputs, i.e., the range profiles of the chaff cloud with plane in the test set, for all possible values of the class label y is calculated. The label of the test range profile is determined by finding the class with the maximum output probability, which can be expressed mathematically as

$$y = \arg\max_{y_i} P(y_i) \prod_{m=1}^{3} P(x_m \mid y_i) \tag{27}$$

The block diagram of these processes is illustrated in Fig.11. If we denote N_{suc} as the number of data with Label 1, and the total number of the samples in the test set is M. The recognition rate R_{rec} is obtained according to (18).

4) METHOD 4: DECISION TREE CLASSIFICATION

Decision tree, which usually mimics human thinking ability while making a decision, is a supervised learning technique that can be used for classification. To predict the classes of the

$$d_1^i = \sqrt{\left(p_1^{tc}(i) - C_1^{plane}\right)^2 + \left(p_2^{tc}(i) - C_2^{plane}\right)^2 + \left(p_3^{tc}(i) - C_3^{plane}\right)^2} \tag{16}$$

$$d_2^i = \sqrt{\left(p_1^{tc}(i) - C_1^{chaff}\right)^2 + \left(p_2^{tc}(i) - C_2^{chaff}\right)^2 + \left(p_3^{tc}(i) - C_3^{chaff}\right)^2} \tag{17}$$

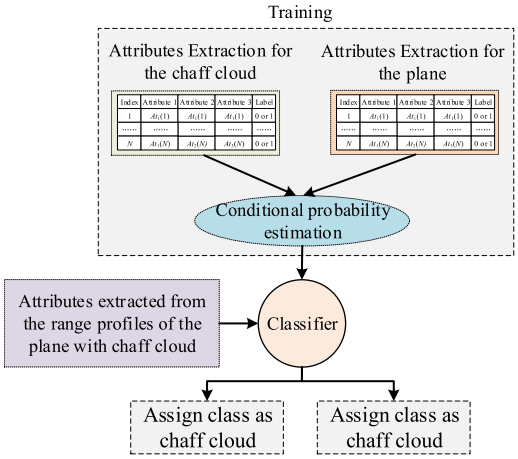

FIGURE 11. The block diagram of Naïve Bayesian classification.

elements in a dataset, the decision tree algorithm compares the attributes of the decision node with that of the elements in the test set. Based on the comparison results, the comparison process follows the branch and jumps to the next node. The principle and the mathematical mechanism of this method are elaborated in [48]–[50].

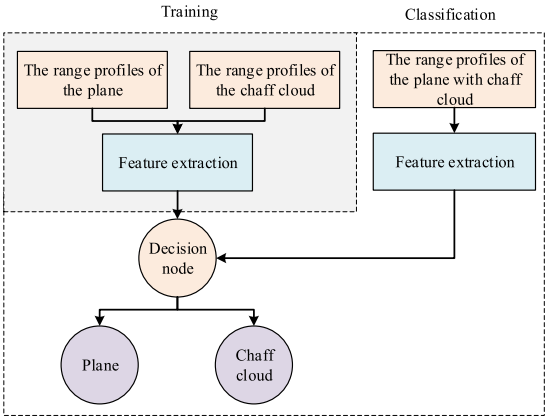

FIGURE 12. The block diagram of the decision tree classification.

Similar to the three methods presented above, the training datasets are formed from the attributes of the range profiles of the plane, say D_1, and chaff cloud, say D_2, respectively. The test dataset is selected as the attributes of the range profiles of the plane with chaff cloud. Meanwhile, the label of set D_1 is assigned as 1, and the label of set D_2 is assigned as 0. The diagram of this method is shown in Fig.12. The attributes of the range profiles are extracted as described in part A of Section III and denoted as (p_i, p_i, p_i) for the i-th sample in the training set. All the attributes and class labels of the range profiles in the training set are listed in a table. The first three columns of the table are filled with the attributes and the fourth column is filled with the class labels. To build a decision tree, the data in the table is sorted in ascending order according to the values in the first column. Then, a splitting index, which divides the data in the table into two parts, can be found based on the maximum information entropy principle. A similar dividing process can be repeatedly performed until all the attributes of the range profile are traversed.

Taking the first column for instance, assume the sample number of the training set is N, a possible dividing index is i_{divide}. The information gain rate is

$$GainRate(col_1) = \frac{Gain(col_1)}{SplitInfo(col_1)} \tag{28}$$

where

$$\begin{aligned} &Info_{col}(i_{divide}) \\ &= -\frac{i_{divide}}{N}\left(\frac{Q_{11}\log_2\frac{Q_{11}}{M_1}}{M_1} + \frac{Q_{21}\log_2\frac{Q_{21}}{M_1}}{M_1}\right) \\ &\quad + \frac{N-i_{divide}}{N}\cdot\left(\frac{Q_{12}\log_2\frac{Q_{12}}{N-i_{divide}}}{N-i_{divide}} + \frac{Q_{22}\log_2\frac{Q_{22}}{N-i_{divide}}}{N-i_{divide1}}\right) \end{aligned} \tag{29}$$

$$\begin{aligned} &Info_{col} \\ &= SplitInfo_{col} \\ &\quad -\left(\frac{(Q_{11}+Q_{12})\log_2\frac{Q_{11}+Q_{12}}{N}}{N} + \frac{(Q_{21}+Q_{22})\log_2\frac{Q_{21}+Q_{22}}{N}}{N}\right) \end{aligned} \tag{30}$$

$$\begin{aligned} &Gain(col_1) \\ &= Info_{col} - Info_{col}(i_{divide}) \end{aligned} \tag{31}$$

The symbols Q_{11} and Q_{21} are the number of the samples labeled with 0 and 1, respectively. Meanwhile, the row index of these samples are less than i_{divide}. Correspondingly, the symbols Q_{12} and Q_{22} denote the number of the samples labeled with 0 and 1, respectively. In addition, the row index of these samples is larger than or equal to i_{divide}. Then, transverse all the division schemes and find out the best one with the maximum information gain rate. Subsequently, the decision tree and the classifiers are obtained after all the columns are scanned. Next, the labels of the elements in the test dataset are determined according to the established decision tree. Finally, the element number N_{suc} with Label 1 in test set is determined. Thus, the recognition rate R_{rec}can be then calculated as (18).

V. MEASUREMENT AND RESULTS

In this section, indoor measurements are performed in the chamber to investigate the jamming performance of two types of the chaff cloud according to the methods mentioned above. We first introduce the measurement facilities and test steps. Then, the range profiles of the plane and the chaff cloud are experimentally accessed. Based on these results, the jamming efficiency and the optimized tactical using strategy of the chaff cloud are proposed. At last of this section, the jamming efficiency of the chaff cloud under the influence of the environmental noise is studied.

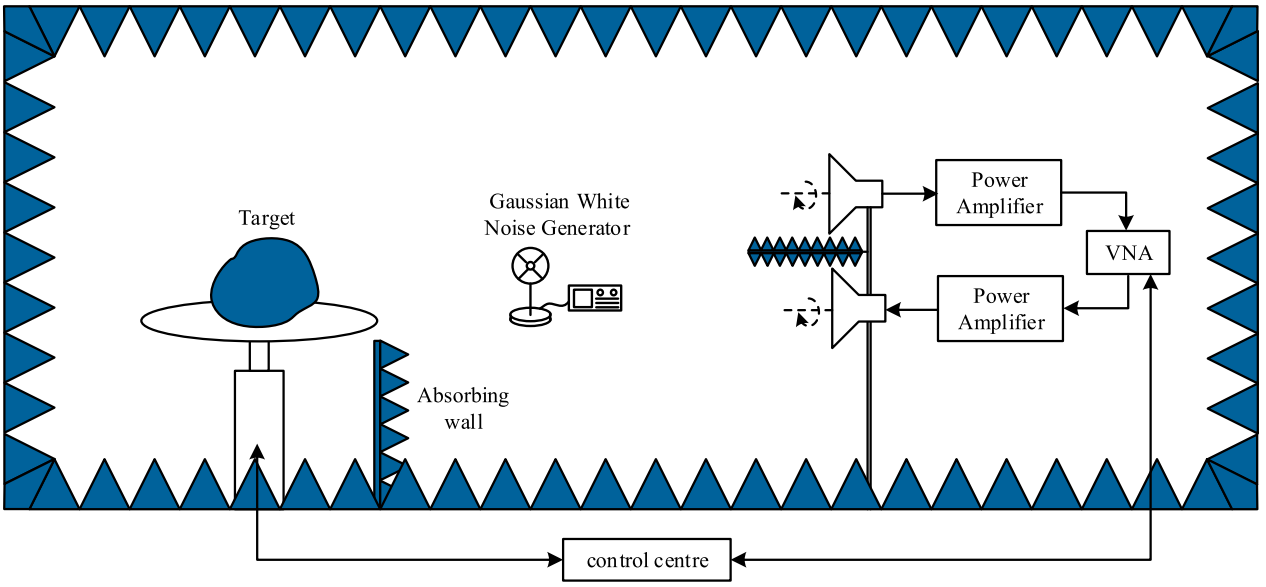

FIGURE 13. The block diagram of the measurement system.

A. INDOOR MEASUREMENT SYSTEM AND STEPS

The range profile measurements of the plane, chaff cloud, and plane with chaff cloud are performed in the radio anechoic chamber in our lab using an SFW measurement system. The test frequencies change from 20 GHz to 24 GHz. The block diagram of the measurement system is shown in Fig.13. A pair of horn antennas are used as the transmitting and receiving devices. To improve the detecting ability of low-reflected power signals, two amplifiers work associating with two antennas. The central computer motivates the vector network analyzer (VNA) and the turntable to change the observation angle and records the corresponding reflected power. The turntable is located on the opposite side of the antennas. The object under test is settled on the upper surface of the turntable. To restrain the EM scattering of the turntable, an absorbing wall is built in front of the turntable. Similarly, an absorbing board is installed between the two antennas for suppressing the direct-transmission noise. For studying the influence of environmental noise on the jamming efficiency of the chaff cloud, a Gaussian white noise generator is placed between the target and the horn antennas. The transmitting power of the generator can be adjusted to simulate the noise of different power intensities. In addition, the transmitting antenna of the noise generator turns towards the receiving antenna of the measurement system.

The range profile measurements are mainly comprised of four steps: Firstly, the measurement system runs about half an hour before the test. Secondly, the vertical heights of the antennas are adjusted to ensure that the centers of the target and the antennas are in the same plane and aligned. Thirdly, the system is calibrated using metallic balls. After this process, all the facilities and variables in the measurement system are fixed. To reduce the multipath effect, the virtual time-domain gating technique is employed. Then, the objects under test (i.e. plane, chaff cloud, and composite model of plane with chaff cloud) are placed on the turntable in turn. The central computer controls the turntable to traverse all the test angles. At each angle, the antennas emit the SFW signal and record the echo. Subsequently, the software provides the EM scattering properties of the object under test at every frequency point and every azimuth angle. These collected data is used to determine the range profiles of the chaff cloud and plane as the method presented in part B of Section II.

B. MEASUREMENTS SETUP

The physical models of the plane (see Fig.14 (a)), chaff cloud (Fig.14 (b) and (c)), and plane with chaff cloud are first made. The geometrical information of these chaff clouds is listed in Table 1. The standard deviations are 0.25, 0.5, 1, 1.5, and 2. The operating frequency of the chaff elements is 22 GHz. It should be noted that the target recognition rates are averaged over 10 samples of the chaff cloud under the same condition. Therefore, Fig.14 just shows one possible physical model of the chaff cloud.

Two types of the chaff clouds are located at different α_c's relative to the plane which are given in Table 2. The chaff cloud models A-1, A-2, and A-3 aim to simulate the plane with the ellipsoid shaped chaff cloud, which is the most common case in practice. The chaff cloud models B-1, B-2, and B-3 aim to describe the scenarios of the plane with the chaff corridor. The test scenarios are shown in Fig.14.

To investigate the influence of the environmental noise on the jamming efficiency of the chaff cloud, a Gaussian white noise generator is located between the target under test and the horn antennas. These three objects form a triangle in the chamber which is shown in Fig.15. The length between the

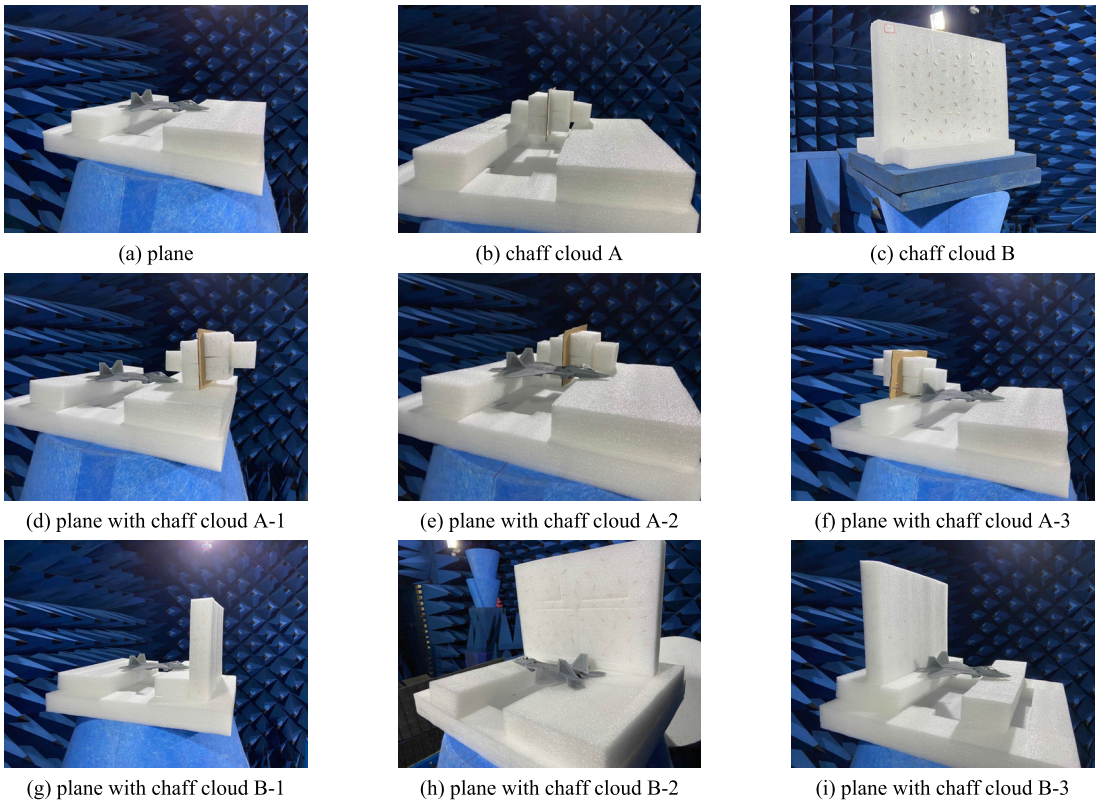

FIGURE 14. The figures of the test scenarios.

TABLE 1. Physical parameters of the chaff cloud.

Case	Shape	Geometric size (cm)	Element length	Elements number
Chaff cloud A	Ellipsoid	20×10×10	0.5 λ	120
Chaff cloud B	Cuboid	40×30×10	0.5 λ	120

TABLE 2. Location parameters of the chaff cloud.

Model index	α_s	Model index	α_s
chaff cloud A-1	0°	chaff cloud B-1	0°
chaff cloud A-2	90°	chaff cloud B-2	90°
chaff cloud A-3	180°	chaff cloud B-3	180°

plane and the antenna $L_1 = 3$ m, the distance between the plane and the Gaussian white generator $L_2 = 2.5$ m, and the distance between the center of two horn antennas and the Gaussian white generator $L_2 = 2.5$ m. The test frequency is also selected at 22 GHz. In this test, only the scenarios of A-1, A-2, B-1, and B-2 are selected. The transmitting power

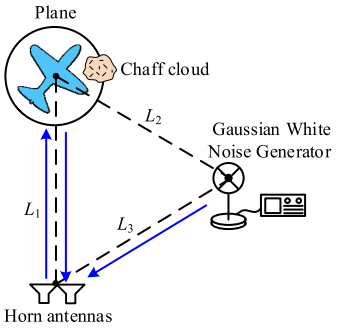

FIGURE 15. The test scenario with a Gaussian white noise background.

of the Gaussian white generator is 0.1, 0.4, and 1.2 times the amplitude of the receiving power of the system with the equitation of the Gaussian white generator. The transmitting antenna of the Gaussian white generator is aligned with the receiving horn antenna. The signal transmission paths of these test scenarios are denoted with the arrows in Fig.15.

C. JAMMING PERFORMANCE ANALYSIS

Utilizing the measurement setups and the facilities in our lab, the range profiles of the plane with chaff cloud A-1, A-2, and A-3 are accessed. The recognition rates are calculated and presented in the first three rows of Tables 3, 4, 5, and 6. The results demonstrate that the recognition rates of the plane

TABLE 3. Recognition accuracy of methods 1.

Model index	Recognition rate (%)		
	Without chaff	With chaff	Decrease
Model A-1	85 %	49 %	36 %
Model A-2	89 %	47 %	42 %
Model A-3	90 %	57 %	33 %
Model B-1	85 %	69 %	16 %
Model B-2	89 %	64 %	25 %
Model B-3	90 %	73 %	17 %

TABLE 4. Recognition accuracy of methods 2.

Model index	Recognition rate (%)		
	Without chaff	With chaff	Decrease
Model A-1	87 %	75 %	12 %
Model A-2	70 %	51 %	19 %
Model A-3	81 %	67 %	14 %
Model B-1	87 %	79 %	8 %
Model B-2	70 %	65 %	15 %
Model B-3	81 %	74 %	7 %

TABLE 5. Recognition accuracy of methods 3.

Model index	Recognition rate (%)		
	Without chaff	With chaff	Decrease
Model A-1	92 %	89 %	3 %
Model A-2	76 %	68 %	8 %
Model A-3	91 %	89 %	2 %
Model B-1	92 %	80 %	10 %
Model B-2	76 %	64 %	12 %
Model B-3	91 %	84 %	7 %

TABLE 6. Recognition accuracy of methods 4.

Model index	Recognition rate (%)		
	Without chaff	With chaff	Decrease
Model A-1	55 %	52 %	3 %
Model A-2	46 %	37 %	9 %
Model A-3	52 %	45 %	7 %
Model B-1	55 %	52 %	3 %
Model B-2	46 %	36 %	10 %
Model B-3	52 %	44 %	8 %

provided by the Euclidean distance classification method are sharply decreased when employing the chaff jamming. While the other three methods show relatively small fluctuations on the recognition rate. The possible reason is that the data regains of two classes in attributes' space are partially overlapped. In addition, the recognition rates of all the four methods are decreased after using the chaff cloud. This result indicates that the chaff cloud can reduce the recognition rates of the plane, and thus increases the survival rate of the plane. Besides, it is found that the chaff cloud which is released near the wings of the plane can achieve a better jamming performance compared with the other releasing locations. The possible reason is that the size of the wing is close to that of the chaff cloud, and the scattering center distribution of the plane on the side aspect is similar to that of the chaff cloud. The influence of environmental noise on the recognition rate of the plane is shown in Tables 7, 8, 9, and 10. It can be found that the recognition rates of the target decrease when the Gaussian noise generator is working. This result indicates that the noise of the environment significantly influences the target recognition. Because the echo of the target is drowned in the environmental noise, which equivalently brings a wide range spatial distributions of the equivalent scattering centers. This confuses the recognition algorithms in extracting the geometric attitudes of the plane. It is also learned from the tables that the recognition rates of the plane decrease sharply with the increasing of transmitting power of the Gaussian noise generator. The recognition rates are even lower than 10 % when the transmitting power of the Gaussian noise generator is 1.2 times the received power without the existence of the noise. The reason is that the geometric information of the plane is completely destroyed by the noise. Thus, according to the results and analysis presented above, we conclude:

(i) The Euclidean distance and decision tree classification methods are not suitable for the target recognition under the chaff jamming. In other words, the chaff cloud can achieve a good jamming performance if the recognition strategies of the radar are based on Euclidean distance or decision tree classification method. Furthermore, the supervised learning algorithms (Methods 2 and 3) have a better performance in anti-interference of the chaff jamming compared with the unsupervised learning algorithm (Method 1). In all these four methods, the SVM classification method achieves the best anti-jamming performance. These facts indicate that the method adopted in the radar system directly affects the jamming performance of the chaff cloud.

(ii) Only from the aspect of data analysis, it is better to release the chaff cloud near the plane wings for realizing a good jamming performance. In actual applications, some planes indeed release the chaff elements from their wings. Nevertheless, this release strategy is hard to form an ellipsoid shaped chaff cloud. Therefore, in practice, most of the planes still release chaff elements from their tails.

(iii) The environmental noise significantly influences the recognition rates of the target. In the sense of confusing radar, the noise together with the chaff cloud enhances the jamming performance. However, in the scenarios of the air campaign, the power level of the environmental noise is quite low compared with the echo power level of the plane. Because the

TABLE 7. Recognition accuracy of methods 1 (with noises).

Model index	Recognition rate (%)							
	Without chaff	With noise			With chaff	With noise		
		0.1	0.6	1.2		0.1	0.6	1.2
Model A-1	85 %	85 %	36 %	2 %	49 %	47 %	32 %	1 %
Model A-2	89 %	88 %	41 %	5 %	47 %	43 %	36 %	4 %
Model B-1	85 %	83 %	39 %	6 %	69 %	66 %	24 %	5 %
Model B-2	89 %	87 %	41 %	3 %	64 %	63 %	31 %	3 %

TABLE 8. Recognition accuracy of methods 2 (with noises).

Model index	Recognition rate (%)							
	Without chaff	With noise			With chaff	With noise		
		0.1	0.4	1.2		0.1	0.4	1.2
Model A-1	92 %	90 %	43 %	3 %	89 %	86 %	36 %	3 %
Model A-2	76 %	74 %	38 %	6 %	68 %	59 %	31 %	2 %
Model B-1	92 %	86 %	39 %	2 %	80 %	73 %	27 %	3 %
Model B-2	76 %	71 %	42 %	3 %	64 %	55 %	26 %	3 %

TABLE 9. Recognition accuracy of methods 3 (with noises).

Model index	Recognition rate (%)							
	Without chaff	With noise			With chaff	With noise		
		0.1	0.4	1.2		0.1	0.4	1.2
Model A-1	87 %	85 %	39 %	2 %	75 %	69 %	26 %	2 %
Model A-2	70 %	68 %	34 %	3 %	51 %	43 %	22 %	1 %
Model B-1	87 %	84 %	36 %	7 %	79 %	68 %	31 %	4 %
Model B-2	70 %	61 %	32 %	6 %	65 %	60 %	27 %	6 %

TABLE 10. Recognition accuracy of methods 4.

Model index	Recognition rate (%)							
	Without chaff	With noise			With chaff	With noise		
		0.1	0.4	1.2		0.1	0.4	1.2
Model A-1	55 %	44 %	15 %	2 %	52 %	43 %	9 %	2 %
Model A-2	46 %	36 %	10 %	3 %	37 %	29 %	5 %	4 %
Model B-1	55 %	49 %	8 %	5 %	52 %	48 %	5 %	1 %
Model B-2	46 %	37 %	13 %	4 %	36 %	29 %	8 %	4 %

electromagnetic background of the plane is clean. When the plane glides near the ground, the environmental noise caused by the ground clutter remarkably increases. This makes the plane harder to be detected. In our experiments, the recognition rates are lower than 10 % in some cases. This means that the jamming efficiency estimation of the chaff

cloud is not available under high power level experimental noise.

Next, let's deal with the range profiles of the plane with chaff corridors B-1, B-2, and B-3. The recognition rates are reported in the last three rows in Tables 3, 4, 5, and 6. Similar to models A-1, A-2, and A-3, the Euclidean distance classification method still shows the worst target recognition performance while the SVM classification method has the best recognition performance. By releasing the chaff corridor at the side of the plane, the lowest recognition rate is reached which is equivalent to the best jamming performance of the chaff cloud. A possible reason for this result is that the chaff corridor blocks the transmission of the EM wave, and the size of the plane on the aspect of the side view is close to the scale of the chaff corridor. Similar to the previous cases, the decision tree classification method still has a poor anti-chaff- jamming ability. Based on the analysis above, we conclude:

(i) The chaff corridor achieves good jamming performance when utilizing the Euclidean distance and the decision tree classification methods to distinguish the target from the chaff jamming. The supervised learning algorithms (Methods 2 and 3) have a better ability in anti-chaff-jamming compared with the unsupervised learning algorithm (Method 1). In all these four methods, the SVM classification method shows its robustness in target recognition under the chaff jamming. Consequently, the target recognition methods equipped in radar system are highly related to the jamming performance of the chaff corridor.

(ii) The chaff corridor should be released near the wing of the plane to form a ''chaff wall'', which achieve a better jamming efficiency. In actual applications, large numbers of chaff elements should be released from the bilateral wings of the plane. Then, the plane migrates behind the chaff corridor for shielding. In addition, the jamming efficiency of the chaff corridor is higher than that of the ellipsoid chaff cloud. Because fewer geometric structures of the plane are exposed within the beam of the radar under chaff corridor jamming compared with the ellipsoid chaff jamming. These presented results also show the validity of the strategies which are adopted in reality.

(iii) Being the same to the ellipsoid chaff cloud, in the case of the chaff corridor, the environmental noise still severely affects the recognition rate of the plane. Besides, this rate decreases with the increasing of the transmitting power level of the Gaussian white noise generator under the conditions of with- or without chaff jamming.

All the results presented above show that both the ellipsoid chaff cloud and the corridor can reduce the target recognition rates. Nevertheless, the recognition algorithms adopted by the radar are extremely influencing the jamming efficiency of the ellipsoid chaff cloud and the chaff corridor. It beyond all doubt that the usage of the chaff cloud when the plane is under attack can increase the survival rate of the plane. Furthermore, the ellipsoid chaff cloud or the chaff corridor which is released near the wings of the plane achieves a better jamming performance.

VI. CONCLUSION

In this paper, the jamming efficiency of elliptical and cubic chaff clouds is estimated. The simulation models of the chaff clouds are firstly established on computer. Then, the physical model of the chaff cloud is made using an elements insertion machine, which ensures the making accuracy of the physical model and provides a new way to produce a physical model that is accurately matched with the simulation one. To consider the complex EM coupling between chaff elements and the coupling between the chaff cloud and the target, the indoor measurements are performed to access the range profiles of the jammer and the plane. Based on the obtained data, three attributes of the range profiles related to the geometric features of the target and the jammer are extracted. Then, four classification methods are used to estimate the target recognition rates of the plane under the chaff jamming, which is used to estimate the jamming performance of the chaff cloud. Results show that the chaff cloud indeed reduces the recognition rates of the plane, and thus improves the survival rate of the target. It is also found that the chaff cloud released on the side of the plane achieves a higher jamming efficiency. Regarding the influence of the environmental noise, the tests are conducted with different transmitting power of the Gaussian noise generator. Results show that the noise can significantly influence the recognition rates of the plane. When the power level of the noise is high enough, the target cannot be detected from the range profile. In future work, more recognition methods will be used to perform further study on the tactical use of the chaff cloud. Meanwhile, outdoor EM scattering evaluation measurements about chaff cloud with a plane can be conducted, and further explorations should be done to obtain the accurate diffusion models of the chaff cloud released by the high-speed carrier.

REFERENCES

[1] Wikia. *Chaff (Countermeasure)*. Accessed: Aug. 9, 2016. [Online]. Available: https://military.wikia.org/wiki/Chaff_(countermeasure)

[2] S. W. Marcus, ''Bistatic RCS of spherical chaff clouds,'' *IEEE Trans. Antennas Propag.*, vol. 63, no. 9, pp. 4091–4099, Sep. 2015.

[3] S. S. Li, Z. Q. Fu, and J. L. Chen, ''Chaff cloud modeling and research on technology of polarization characteristic simulation,'' *J. Projectiles Rockets Missiles Guid.*, vol. 4, no. 36, pp. 157–160, Jun. 2016.

[4] X. Shao and H. Du, ''Echo theoretical analysis from chaff cloud and research polarization targets recognition,'' in *Proc. Int. Conf. Microw. Millim. Wave Technol.*, Builin, China, Apr. 2007, pp. 1–5.

[5] H. U. Shou-Jun, ''Chaff induction current distribution and scattering characteristics,'' *Electro-Opt. Technol. Appl.*, vol. 24, no. 3, pp. 23–27, Jun. 2009.

[6] X. B. Yang and S. W. Lv, ''Backscattering cross section of chaff clouds,'' *Acta Aeronautica Et Astronautica Sinica*, vol. 19, no. S1, pp. 82–84, Dec. 1998.

[7] S. Q. Chen and Q. Cai, ''Morn calculation of back scattering RCS for thin chaff wire,'' *Comput. Telecommun.*, vol. 2012, no. 3, pp. 59–61, Jun. 2012.

[8] S. G. Li, ''Study on motion and scatter model of outer space chaff,'' M.S. thesis, School Electron. Eng., Xidian Univ., Xi'an, China, 2015.

[9] J. Cheng, "The scattering characteristics of novel chaff and foil," M.S. thesis, School Electron. Sci. Technol., Graduate School Nat. Univ. Defense Technol., Changsha, China, 2015.
[10] Y. Liu, Z. J. Gu, and Z. P. Sun, "Research on motion model of chaff cloud in radio frequency simulation system," *J. Syst. Simul.*, vol. 26, no. 3, pp. 513–516, Mar. 2014.
[11] T. A. Winchester, "Pulsed radar return from a chaff cloud," *IEE Proc. F Radar Signal Process.*, vol. 139, no. 4, pp. 315–320, Aug. 1992.
[12] Z.-W. Wang, H. Wang, C. Zhang, D. Y. Xie, and H. L. Jin, "Experimental study of distribution of chaff cloud launched at high-speed," *Acta Armamentarii*, vol. 38, no. 6, pp. 1075–1081, Jun. 2017.
[13] X. W. Yan, "A novel anti-chaff-jamming method based on geometrical inference matching algorithm," *Signal Process.*, vol. 11, no. 17, pp. 98–113, Nov. 2010.
[14] Z. Hong, P. Yu-Jian, W. Qing-Ping, T. Ning, and Y. Naichang, "An anti-chaff jamming method for millimeter wave wideband coherent radar based on range Doppler feature," in *Proc. IEEE Int. Conf. Signal Process., Commun. Comput.*, Ningbo, China, Sep. 2015, pp. 1–6.
[15] C. Gan, K. Zhang, and Y. J. Li, "Tactical application research of chaff corridor," *Fire Control Command Control*, vol. 33, no. 7, pp. 44–47, Jul. 2008.
[16] P. T. Dung, "Combined neural networks for radar target recognition from radar range profiles," in *Proc. Int. Conf. Adv. Technol. Commun.*, Hanoi, Vietnam, Oct. 2008, pp. 353–355.
[17] S. Luo and S. Li, "A novel approach of automatic target recognition using high resolution radar range profiles," in *Proc. Int. Symp. Microw., Antenna, Propag. EMC Technol. Wireless Commun.*, Hangzhou, China, Aug. 2007, pp. 852–855.
[18] L. Li and Z. Liu, "Radar high resolution range profile recognition via dual-SVDD classifier," in *Proc. CIE Int. Conf. Radar (RADAR)*, Guangzhou, China, Oct. 2016, pp. 1–4.
[19] B. Bati and N. Duru, "Sequential naval target range profile classification using special fusion method," in *Proc. 4th Int. Conf. Comput. Sci. Eng. (UBMK)*, Samsun, Turkey, Sep. 2019, pp. 475–477.
[20] J. Lu, Z. Xi, X. Yuan, G. Yu, and M. Zhang, "Ship target recognition using high resolution range profiles based on FMT and SVM," in *Proc. IEEE CIE Int. Conf. Radar*, Chengdu, China, Oct. 2011, pp. 1299–1302.
[21] L. Long, S. Tao, and S. Zhengbo, "Size estimation of space target using cross-range profile," in *Proc. 3rd Int. Conf. Comput. Sci. Netw. Technol.*, Dalian, China, Oct. 2013, pp. 1143–1147.
[22] Y. Zhu, H. Zhao, Q. Fu, and D. Le, "Stepped-frequency range profiling of multiple overlapped targets," in *Proc. IEEE Radar Conf.*, Rome, Italy, May 2008, pp. 1–4.
[23] H. Huang, Z. Tong, S. Chai, and Y. Zhang "Experimental and numerical study of chaff cloud kinetic performance under impact of high speed airflow," *Chin. J. Aeronaut.*, vol. 31, no. 11, pp. 27–39, Sep. 2018.
[24] Y. L. Guo, J. W. Wan, J. P. Ou, and F. B. Chen "Research on anti-chaff jamming method based on range profile," *Radar Sci. Technol.*, vol. 9, no. 1, pp. 67–71, Jan. 2011.
[25] J. Wan, B. Chen, B. Xu, H. Liu, and L. Jin, "Convolutional neural networks for radar HRRP target recognition and rejection," *EURASIP J. Adv. Signal Process.*, vol. 2019, no. 1, pp. 1–17, Dec. 2019.
[26] K. Schuler and W. Wiesbeck, "Extraction of scattering centers of vehicles by ray-tracing simulations," in *Proc. 4th IASTED Int. Conf. Antennas, Radar Wave Propag.*, Montreal, QC, Canada, 2007, pp. 132–136.
[27] B. Pei and Z. Bao, "Multi-aspect radar target recognition method based on scattering centers and HMMs classifiers," *IEEE Trans. Aerosp. Electron. Syst.*, vol. 41, no. 3, pp. 1067–1074, Jul. 2005.
[28] J. H. Yi, B. Bhanu, and M. Li, "Target indexing in SAR images using scattering centers and the Hausdorff distance," *Pattern Recognit. Lett.*, vol. 17, no. 11, pp. 1191–1198, Sep. 1996.
[29] A. L. Wang, Z. F. Shi, and A. Zhang, "Model and application to target recognition of based on entropy," *Fire Control Command Control*, vol. 30, no. 2, pp. 110–112, Feb. 2012.
[30] L. C. Potter and R. L. Moses, "Attributed scattering centers for SAR ATR," *IEEE Trans. Image Process.*, vol. 6, no. 1, pp. 79–91, Jan. 1997.
[31] J. Wang and N. Yu, "Multi-target tracking via max-entropy target selection and heterogeneous camera fusion," in *Proc. Adv. Multimedia Inf. Process. Multimedia*, Gwangju, South Korea, 2015, pp. 149–159.
[32] M. Y. Bai, Y. Ding, and Z. W. Hu, "PHD multi-target tracking based on entropy penalized EM of unknown clutter estimation," *Electron. Opt. Control*, vol. 4, no. 13, pp. 49–56, Apr. 2011.
[33] Z. Yanchun, L. Chunyong, G. Lixin, and L. Songhua, "Evaluation of efficient dielectric constants of chaff corridor in submillimeter band," in *Proc. Int. Conf. Microw. Millim. Wave Technol. (ICMMT)*, Guangzhou, China, May 2019, pp. 1–3.
[34] S. I. Gass and M. C. Fu, *Acceptance-Rejection Method*. Boston, MA, USA: Springer, 2013, pp. 81–153.
[35] E. Bach, "Efficient prediction of Marsaglia–Zaman random number generators," *IEEE Trans. Inf. Theory*, vol. 44, no. 3, pp. 1253–1257, May 1998.
[36] J. L. Pinchot, O. Bechu, and P. Pouliguen, "A chaff cloud modelisation," in *Proc. 11th Int. Symp. Antenna Technol. Appl. Electromagn.*, St. Malo, France, Jun. 2005, pp. 1–4.
[37] N. Cam and P. Joongsuk, *Stepped-Frequency Radar Sensors: Theory, Analysis and Design*. New York, NY, USA: Springer, 2016, pp. 25–101.
[38] R. Yang, H. Li, S. Li, P. Zhang, L. Tan, X. Gao, and X. Kang, *Stepped-Frequency Waveform and SAR Imaging*. Singapore: Springer, 2017, pp. 119–157.
[39] R. C. Xu, C. J. Liu, and Z.-P. Chen, "The study of method of range profile feature extraction and recognition," *Radar Sci. Technol.*, vol. 3, no. 5, pp. 262–265, Oct. 2005.
[40] J. B. Keller, "Geometrical theory of diffraction," *J. Opt. Soc. Amer.*, vol. 52, no. 2, pp. 116–130, Feb. 1962.
[41] A. E. Abbas, "Entropy," *Wiley Encyclopedia Biomed. Eng.*, vol. 2, no. 2, pp. 70–77, Dec. 1967.
[42] A. Bhensle and R. Raja, "An efficient face recognition using PCA and Euclidean distance classification," *Int. J. Comput. Sci. Mobile Comput.*, vol. 3, no. 6, pp. 407–413, Jun. 2014.
[43] G. M. Foody and A. Mathur, "Toward intelligent training of supervised image classifications: Directing training data acquisition for SVM classification," *Remote Sens. Environ.*, vol. 93, nos. 1–2, pp. 107–117, Oct. 2004.
[44] P. Hao, J. Chiang, and Y. Tu, "Hierarchically SVM classification based on support vector clustering method and its application to document categorization," *Expert Syst. Appl.*, vol. 33, no. 3, pp. 627–635, Oct. 2007.
[45] J. Vaidya, H. Yu, and X. Jiang, "Privacy-preserving SVM classification," *Knowl. Inf. Syst.*, vol. 14, no. 2, pp. 161–178, Mar. 2007.
[46] H.-J. Huang and C.-N. Hsu, "Bayesian classification for data from the same unknown class," *IEEE Trans. Syst., Man, Cybern. B, Cybern.*, vol. 32, no. 2, pp. 137–145, Apr. 2002.
[47] R. Hanson, J. Stutz, and P. Cheeseman, "Bayesian classification theory," NASA Ames Res. Center, Mountain View, CA, USA, Tech. Rep. FIA-90-12-7-01, Nov. 1991.
[48] A. Srivastava, E.-H. Han, V. Kumar, and V. Singh, "Parallel formulations of decision-tree classification algorithms," in *Proc. Int. Conf. Parallel Process.*, Minneapolis, MI, USA, 1998, pp. 237–244.
[49] M. A. Friedl and C. E. Brodley, "Decision tree classification of land cover from remotely sensed data," *Remote Sens. Environ.*, vol. 61, no. 3, pp. 399–409, Sep. 1997.
[50] A. Dobra, *Decision Tree Classification*. Boston, MA, USA: Springer, 2009, pp. 765–769.

YANCHUN ZUO received the B.E. degree from Xinyang Normal University, Xinyang, China, in 2013, and the M.E. degree from Xidian University, Xi'an, China, in 2014, where he is currently pursuing the D.E. degree in electromagnetic field and microwave technology.

He has published four papers in conference proceedings. His main research interests include electromagnetic scattering modeling and scattering measurements.

LIXIN GUO (Senior Member, IEEE) received the M.S. degree in radio science from Xidian University, Xi'an, China, in 1993, and the Ph.D. degree in astrometry and celestial mechanics from the Chinese Academy of Sciences, China, in 1999.

From 2001 to 2002, he was a Visiting Scholar with the School of Electrical Engineering and Computer Science, Kyungpook National University, Daegu, South Korea. He has also been a Visiting Professor with the d'Energetique des Systemes et Precedes (LESP), University of Rouen, Mont-Saint-Aignan, France, and the Faculty of Engineering and Physical Sciences, The University of Manchester, Manchester, U.K. Since 2018, he has been a Chief Professor with the Innovative Research Team, Ministry of Science and Technology, China. He is currently a Professor and the Head of the School of Physics and Optoelectronic Engineering, Xidian University. He has authored or coauthored six books and over 300 journal articles. He has been in charge of and undertaken more than 30 projects. His research interests include electromagnetic wave propagation and scattering in complex and random media, computational electromagnetics, inverse scattering, and antenna analysis and design.

Dr. Guo was a Fellow of the Chinese Institute of Electronics (CIE). He was a recipient of the National Science Fund for Distinguished Young Scholars, in 2012, and a Distinguished Professor of Changjiang Scholars Program, in 2015. He was the Vice President of the Physics Institute of Shaanxi Province, China.

WEI LIU (Member, IEEE) received the M.S. degree in mechanical engineering and automation and the Ph.D. degree in radio science from Xidian University, Xi'an, China, in 2003 and 2013, respectively.

He is currently an Associate Professor of physics and optoelectronic engineering with Xidian University, China. His research interests include electromagnetic wave propagation and scattering in complex and random media, and computational electromagnetics.

JIANYANG DING (Graduate Student Member, IEEE) received the B.E. degree from Xidian University, Xi'an, China, in 2018, where he is currently pursuing the Ph.D. degree in indoor positioning with the School of Telecommunications Engineering. His current research interests include wireless communication and signal processing.